New Si–Cu and Si–Ni anode materials for lithium-ion batteries

Alexander Y. Galashev & Yuri P. Zaikov

Journal of Applied Electrochemistry

ISSN 0021-891X
Volume 49
Number 10

J Appl Electrochem (2019) 49:1027-1034
DOI 10.1007/s10800-019-01344-9

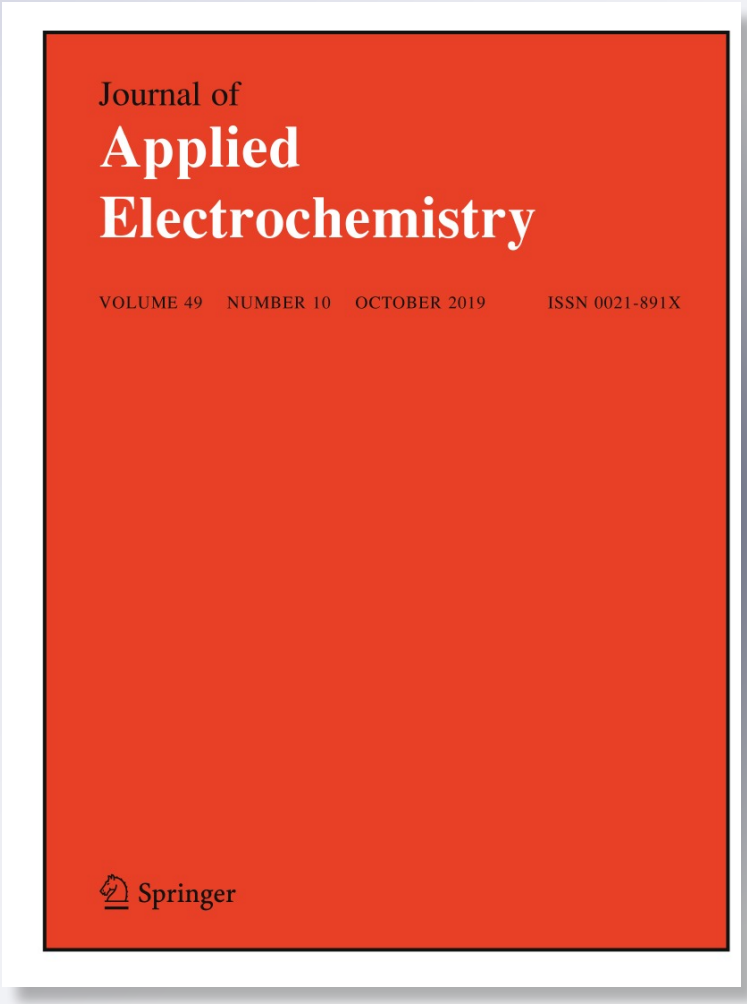

Springer

Journal of Applied Electrochemistry (2019) 49:1027–1034
https://doi.org/10.1007/s10800-019-01344-9

RESEARCH ARTICLE

New Si–Cu and Si–Ni anode materials for lithium-ion batteries

Alexander Y. Galashev[1,2] · **Yuri P. Zaikov**[1,2]

Received: 15 May 2019 / Accepted: 31 July 2019 / Published online: 22 August 2019

Abstract

The functioning of the new anode materials in the form of silicene on copper and nickel substrates was tested by the method of molecular dynamics. It is shown that, two-layer silicene, both ideal and with vacancy defects, on Cu (111) and Ni (111) substrates is more preferable for intercalation of lithium than the corresponding material on Ag (111) substrate. In turn, a higher capacity was found for a lithium-filled silicene channel on a nickel substrate than for a corresponding anode on a copper substrate. In addition, local shear stresses in a functioning silicene anode on a Ni (111) substrate are lower than those on a Cu (111) substrate.

Graphic abstract

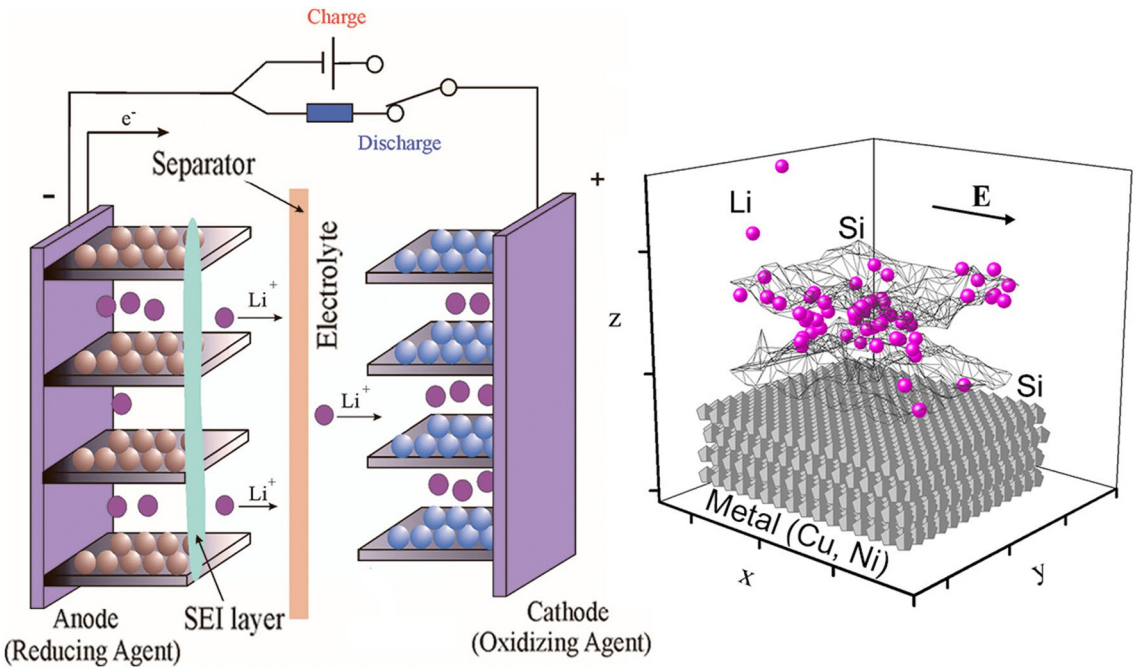

Keywords Copper · Lithium ion · Molecular dynamics · Nickel · Silicene · Stress

1 Introduction

The development of lithium-ion batteries (LIB) in the near future may create conditions for their widespread use in electric vehicles. To do this, it is necessary to meet significantly higher requirements for both energy and power. In

Electronic supplementary material The online version of this article (https://doi.org/10.1007/s10800-019-01344-9) contains supplementary material, which is available to authorized users.

✉ Alexander Y. Galashev
galashev@ihte.uran.ru

Extended author information available on the last page of the article

transport batteries currently used, it is necessary to replace both electrodes and combustible organic electrolytes. The anode material in the form of silicene on a copper or nickel substrate is designed for lithium-ion batteries. In the last two decades, various cathode materials have been introduced for the lithium-ion battery. Among them are lithium-nickel oxide, lithium-manganese oxide, and lithium-iron-phosphate. However, graphite is still used as anode material. The graphite anode has a non-high theoretical capacity (~ 372 mAh g^{-1}), which is 10 times less than the capacity of metallic lithium (3800 mAh g^{-1}). In addition, when performing the first cycle, there is an irreversible loss of capacity of the graphite anode. Among the materials that could be suitable for the manufacture of the anode, stand out silicon and tin. Their theoretical energy densities are 4190 and 990 mAh g^{-1}, respectively. The reason that such anodes still have not found use lies in their large swelling during lithium intercalation. The formation of an alloy between Li and Si is characterized by the reaction

$$4.4\mathrm{Li} + \mathrm{Si} \rightarrow \mathrm{Li}_{4.4}\mathrm{Si} \quad (1)$$

Tin can form with lithium an intermetallic compound composition of which is similar to that reflected by reaction (1), i.e., there can be 4.4 Li atoms per Sn atom. However, along with this intermetallic compound, tin forms a number of other compounds, in which a smaller number of Li atoms are found per one tin atom [1]. An almost fourfold increase in the volume of Si is accompanied by the appearance of strong stresses in the electrode, because of which internal cracks appear. Ultimately, when cycling, this leads to the crumbling of the electrode. Electrode crumbling results in loss of electrical contact and an increase in impedance. Because of this, the electrode becomes unusable.

Attempts have been made to eliminate large volume changes in lithiation using nanoparticles, porous structures, nanocomposites, and thin Si films, including films with a protective graphene shell that enhances electric and mechanical properties [2]. In addition to massive volume expansion, Si anodes were characterized by low conductivity and the formation of unstable solid electrolyte interphase (SEI) layers. It was shown that for satisfactory practical use, the size of Si particles in a Si/carbon nanocomposite should be less than 150 nm [3]. However, in the case of that study, there were some drawbacks which reduce the efficiency of the battery. In particular, the SEI remained unstable. The sandwich-structured silicon thin film anodes should allow to largely eliminating the unacceptable electrochemical and mechanical degradation [4]. A stable film of SEI on the electrode can be provided by the sandwich from silicon thin film with lithium phosphorus oxynitride (LiPON) [5].

The development of proper anode material is still a challenge for the production of a new generation of ion batteries. The improvements made for anodes with lithium [6], as well as sodium and potassium [7] charge carriers, did not lead to a significant increase in the capacitance of the electrode. As an anode, it was proposed to use 3D Si structures formed on the patterned copper current collectors. However, this design only slightly improves the cycling characteristics without sufficiently extending the life of the anode [8].

The need for efficient energy storage and transformation devices is steadily increasing. The leading place among these devices is taken by supercapacitors, which are reliable and safe and have a high power density, and high charge–discharge rate [9]. As the electrode materials, many oxides and nitrides of transition metals were tested [10, 11]. However, it is very difficult for these materials to produce an effective current collection. Their practical application was negated due to the larger contact resistance and high stiffness in the joint [12]. Recently, an increasing preference has been given to electrodes in the form of electroactive nanostructures deposited on electrically conductive substrates. Such electrodes are ideally suited for the development of new flexible LIB [13]. Graphene-based flexible electrodes have a high surface-to-volume ratio. In addition to flexibility, they have a lightweight, better electrical conductivity, and own two-layer capacity. Similar silicene-based electrodes using highly conductive metal substrates, in addition to these qualities, will have a much higher electrical capacitance. This makes the nanocomposite material, "silicene on a metal substrate," the most promising candidate for use in flexible lithium-ion batteries.

This article is devoted to the development of a new anode material with a high specific capacity, which is a silicene-copper or silicene-nickel nanocomposite.

2 Materials and methods

A silicene channel located on metallic Cu (111) or Ni (111) substrates represented the anode in the model. The silicene channel was formed by two silicene sheets with a size (x, y) of each of them 4.8×4.1 nm. Each sheet consisted of 300 Si atoms. The silicene unit cell contained 18 atoms, 6 (selected in a certain way) of which raised above the main plane at a distance of 0.064 nm. Such a flower structure was observed experimentally in silicene obtained on an Ag (111) substrate [14]. The substrate overlying silicene in each of the directions (x and y) was formed from four (111)—layers of a copper or nickel crystal and contained 1536 atoms. Initially, the distance between the lower sheet of silicene and the upper layer of the substrate was 0.26 nm, i.e., corresponding to the optimal value obtained in the DFT calculation [15]. The lithium ions were launched into the channel alternately, one after the other, at regular intervals (10 ps). It is known that, unlike graphite in silicon, an elementary lithium particle is in the form of a neutral atom, and not as

a charged particle, i.e., ion [16]. During the lifetime of the Li^+ ion in the silicene channel (10 ps), it, as a rule, finds an energetically favorable arrangement. The ion is fixed in this position, and further, during the remaining intercalation time (and some deintercalation time), exists as an atom. During the time interval of 10 ps, it seems possible to calculate the kinetic and mechanical (stress tensor) properties of the system for a given number of particles (atoms). In order for the calculations to be correct, each time when the number of atoms in the system changes, these calculations are performed again.

The initial location of the ions was chosen randomly on a line drawn on the frontal plane ($x0z$ at $x=0$) parallel to the $0y$ axis at a distance $h_g/2$ from each of the silicene sheets, where $h_g=0.75$ nm is the gap between the silicene sheets (channel height). The lithium ion had a positive electric charge equal to an elementary electric charge. A constant electric field acting along the $0x$ direction carried the ion inside the channel. The electric field strength during the intercalation of ions was chosen to be equal to 10^3 V/m, and during deintercalation—10^5 V/m. The field strength range of 10^3–10^4 V/m is used to charge modern compact lithium-ion batteries.

The configuration of the "Ni–Si–Li" system, referring to a time point of 500 ps at the filling by lithium of the channel formed by sheets of perfect silicene, is shown in Fig. 1. During this time, 50 lithium ions were introduced into the channel. All intercalating Li atoms are visible in the figure, because silicene sheets are shown as transparent. A significant part of Li atoms is located on the outer surface of the strongly deformed silicene sheets. They can reach there through the gaps between the impermeable sidewalls (not shown in the figure) and the edges of the sheets. It is obvious that a majority of Li atoms belong to the upper sheet.

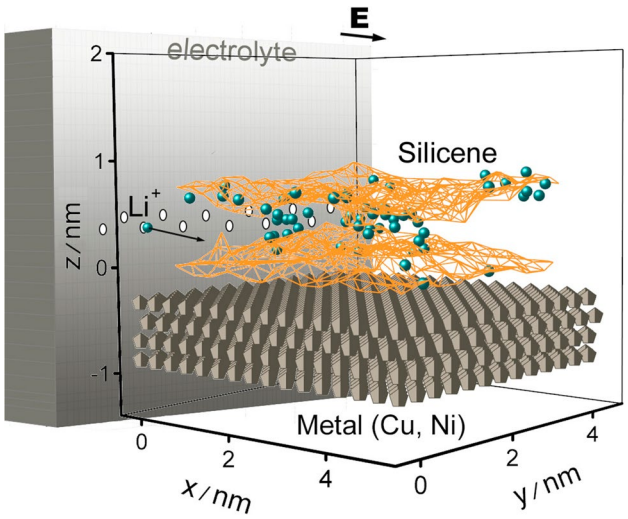

Fig. 1 The channel formed by perfect silicene sheets on a nickel substrate after the intercalation process with lithium

The deintercalation in the silicene channel was also performed sequentially, but in reverse order. In other words, the last of the remaining ions during intercalation left the channel first and so on. Moreover, the time allotted to the ion to exit the channel was 20 ps. During this time, the ion always left the channel. In the channels under consideration, the behavior of Li^+ ions during intercalation and deintercalation was generally similar to the passage of these processes in the silicon channel on the Al (111) substrate [17].

3 Calculation

Molecular dynamics (MD) calculations were performed using the LAMMPS program [18], using parallel computations. The time step of integrating the equations of motion of 0.1 fs allowed us to carry out correct calculations in the NVT ensemble at $T=300$ K without heating the system.

When using the LAMMPS program, the system should not lose particles during the calculation, i.e., none of the atoms must go beyond the rectangular container. Such a container was created using the imposed force field. At the initial moment of time, the distance from any Si or Cu atom to the nearest container wall was not less than 0.5 nm, and the distance from Si atoms of the upper sheet of silicene to the upper wall of the container was 1.15 nm. Li^+ ions (or Li atoms) interacted with the wall only when they approached it at a distance of $r<R_{cutoff}=0.25$ nm. This interaction occurred in accordance with the Lennard-Jones potential (12–6) with parameters $\sigma=0.1$ nm, $\varepsilon=1$ eV. These parameters do not correspond to any real material. They are chosen empirically in order to obtain an adequate model for studying the processes of intercalation/deintercalation. When the distance to the wall was less than 0.1 nm, the repulsive force acting from the wall pushed the atom (ion) back to the system.

The method of statistical geometry is a powerful tool in the structural analysis of mainly irregular packing of various entities, including those located in a limited space. This method consists in dividing the three-dimensional space between entities. Each entity is assigned a certain portion of the space in the shape of a Voronoi polyhedron (VP) [19, 20]. In a restricted system, such as a channel filled with Li atoms, VPs were built only when at least one Li atom was in each half-space considered around the selected center (Li atom).

Our method for calculating the stress distribution in silicene sheets is as follows. We divide the sheets of silicene into elementary areas with the normal γ (x, y, z) and elongated either in the "armchair" direction or in the "zigzag" direction. Next, the resulting force acting on each of the

areas is determined. In determining the resultant force, only those interactions between particles i and j are taken into account, the force vector of which pierces the given area [21]. In addition, the calculation of $\sigma_{\gamma\alpha}(l)$ takes into account the directions α (x, y, z) of the velocities of the atoms i and j:

$$\sigma_{\gamma\alpha}(l) = \left\langle \sum_{i}^{n} \frac{1}{\Omega}\left(m v_{\gamma}^{i} v_{\alpha}^{i}\right)\right\rangle + \frac{1}{S_l}\left\langle \sum_{i}^{n} \sum_{j\neq i}^{(u_i\leq u, u_j\geq u)} \left(f_{ij}^{\alpha}\right)\right\rangle \quad (2)$$

In expression (2), the following notation is used: n is the number of atoms on the lth area, Ω is the volume per atom, m is the atomic mass, v_{α}^{i} is the α projection of the velocity of the ith atom, S_i is the area of the lth surface element, f_{ij}^{α} is the α projection of the force resulting from the interaction of i and j atoms and passes though the lth area, and u_i is the coordinate of the atom i; the symbol u denotes the coordinate of the contact point of the straight line through the centers of the atoms i and j and the lth surface element.

4 Results and discussion

Table 1 shows the comparison of the filling of the same silicene channel located on Ag (111), Cu (111), and Ni (111) substrates with lithium. Moreover, the channel could have walls formed by perfect silicene, as well as silicene, filled with defects: mono-, bi-, and trivacancies. On average (not relative to the presence of defects in silicene and their types), in the presence of a copper substrate, the amount of intercalating lithium increases by 0.7%, and when a nickel substrate is used, it increases by 10.6% relative to the Ag (111) substrate. In this regard, the nickel substrate is preferable to both silver and copper. A positive factor is also the fact that the maximum filling of the channel with lithium on the Ni (111) substrate is achieved in the presence of monovacancies in silicene. On Ag (111) and Cu (111) substrates, this occurs when the silicene contains tri- and bi-vacancies, respectively. With the increasing size of defects, the mechanical stability of silicene decreases, and a channel with such

Table 1 The limit number of lithium atoms intercalating into perfect and defective silicene channels on silver, copper, and nickel substrates

Vacancy type in silicene sheets	Substrate type		
	Silver	Copper	Nickel
Perfect	39	48	74
Monovacancies	51	67	91
Bivacancies	71	86	41
Trivacancies	79	60	60

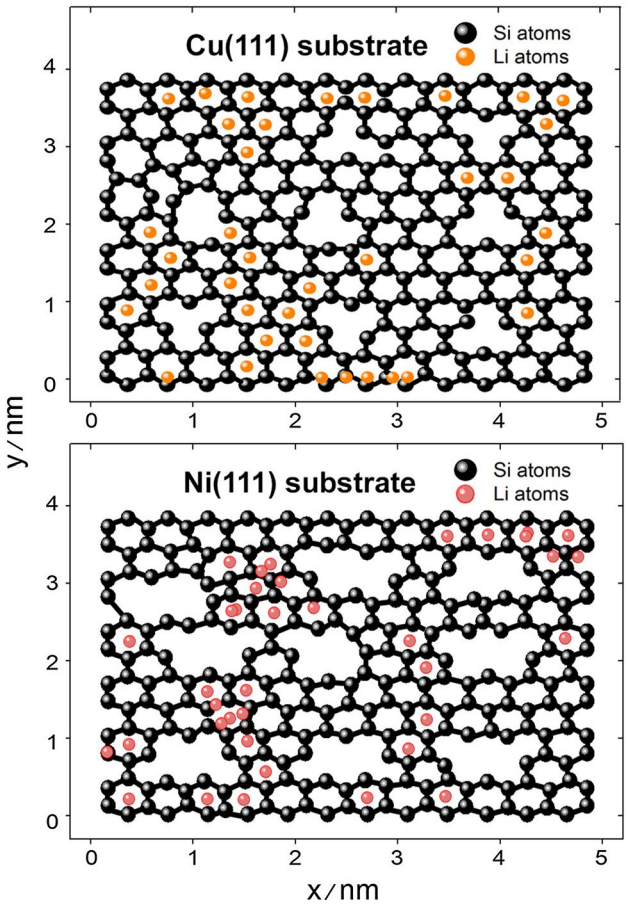

Fig. 2 The xy projections of the upper sheet of silicene with mono- and trivacancies on the Cu(111) and Ni(111) substrates, respectively, at the instant of complete lithiation

Table 2 Changes (in %) in the channel volume (relative to the initial state before filling the channel with lithium) at its maximum filling with lithium and after complete lithium deintercalation in the silicene channels on copper and nickel substrates

(111) substrate	Process direction	Type of vacancy defects			
		Perfect	Monovacancies	Bivacancies	Trivacancies
Cu	Intercalation	+4.2	−13.4	−19.1	−14.6
	Deintercalation	+8.82	−1.96	+2.4	+2.3
Ni	Intercalation	−21.8	−10.3	−2.8	−7.3
	Deintercalation	−5.8	+2.34	+2.28	−21.6

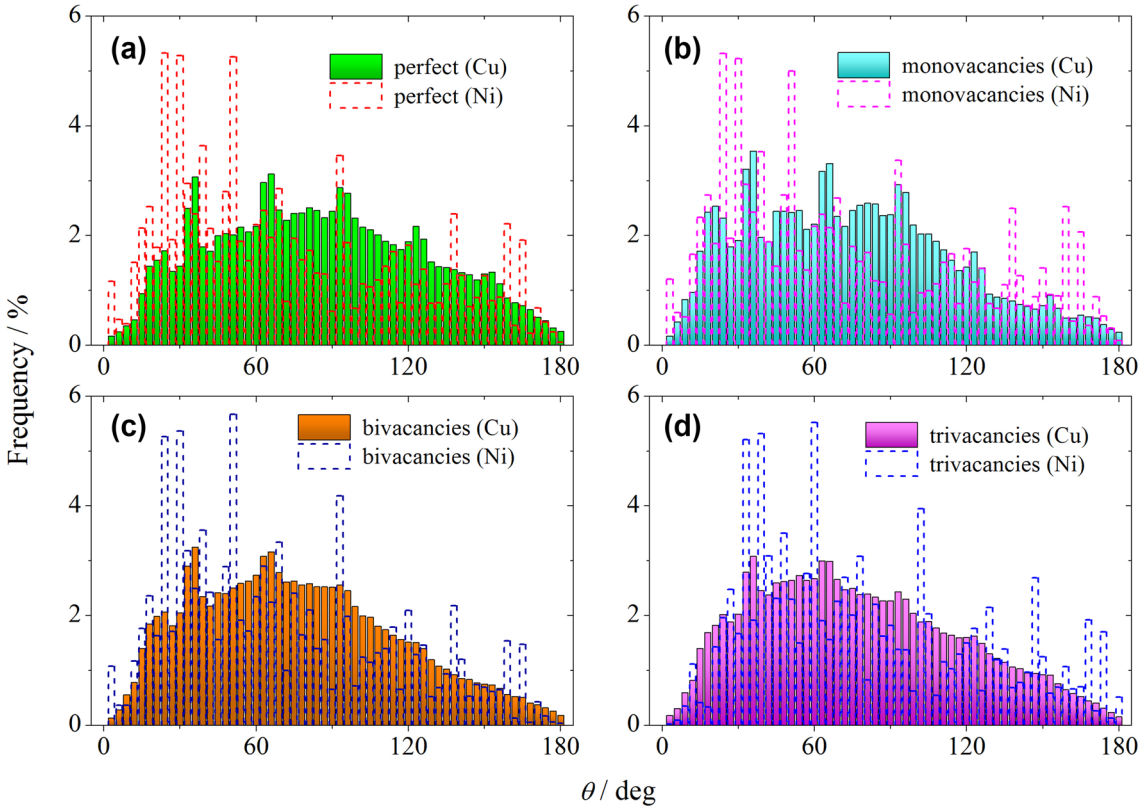

Fig. 3 Angular distributions of the nearest geometric neighbors for packings of Li atoms, corresponding to the limiting filling of silicene channels on copper and nickel substrates. Captions in the margins of the Figure inform the type of vacancies in silicene and the substrate material (in brackets)

walls undergoes more rapid destruction during cycling than a channel with walls containing monovacancies.

Table 2 shows the changes in the volume of the silicene channel at the end of the intercalation and deintercalation processes, when the channel was placed on copper and nickel substrates. After intercalation, a reduction in the volume of the channel is usually achieved, which is associated with its significant deformation and the attractive effect created by lithium filling up the channel. Only for a channel with perfect walls on a copper substrate, a slight (4.2%) increase in its volume was observed after the completion of intercalation. The number of intercalating Li atoms (48 (Cu) vs. 74 for the nickel substrate) in this case also turns out to be small. After deintercalation, the volume of the channel may either increase (as a rule, by a small amount) or remain smaller than the initial one (before intercalation). The channel with monovacancies on the Ni (111) substrate has a moderate reduction (10.3%) of volume after intercalation of 91 Li atoms. It is also characterized by a very small (2.34%) increase in volume after deintercalation. Thus, the use of a channel with monovacancies in this case is preferable not only because of the maximum capacity reached during lithium intercalation, but also because of the good recovery of its volume during cycling.

The *xy* projections of the upper layer of the channel cut by the mean ($z = h_g^*/2$) plane are shown in Fig. 2. The view is given from the side of the plane $z = h_g^*/2$. Here, h_g^* is the vertical channel size after intercalation of lithium. The shape of defects, especially trivacancies, is somewhat better preserved in the top sheet. In the bottom sheet, some trivacancies have adjacent smaller defects. Such defects are five-link, seven-link, and eight-link rings. The upper and lower parts of the channel have approximately equal volumes, but the numbers of Li atoms in them are different: with 37 Li atoms present in the upper part and 30 Li atoms present in the lower part, when the channel was located on a Cu (111) substrate. In the case of using Ni (111) substrate separated by a conditional horizontal plane passing through the midpoint of the initial gap, the lithium atoms were distributed as follows: 37 Li were based near the top sheet and only 23 near the bottom sheet. We notice that a significant portion of Li atoms is located above the centers of the hexagonal rings formed by the Si atoms of both the upper and lower sheets. Near each sheet, there are also local clusters of Li

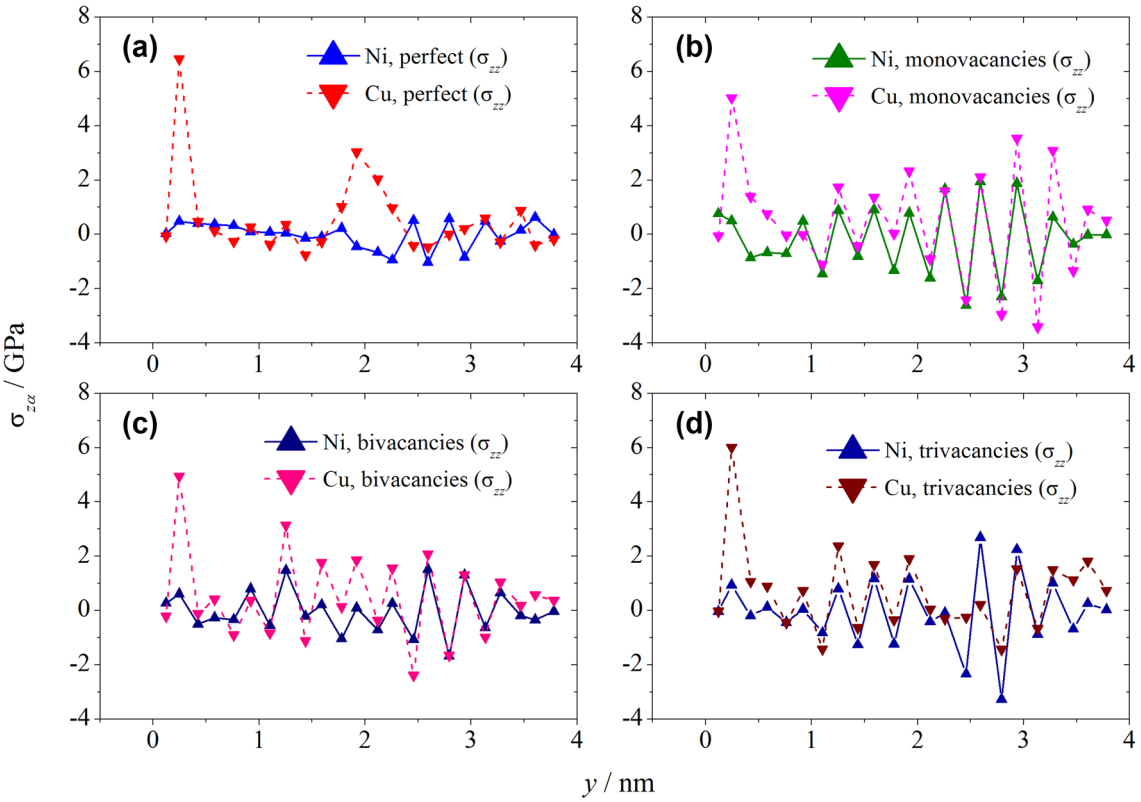

Fig. 4 The distribution of the average σ_{zz} stresses in the sheets of silicene along the *oy* (armchair) direction when lithium is intercalated in a silicene channel located on Ni(111) and Cu(111) substrates. Elementary platforms are elongated along the axis *ox*. The types of defects in silicene and the stresses in question (in parentheses) are indicated in the captions in the margins of figures (a)–(d)

atoms. There is a significant irregularity in the distribution of lithium atoms over the area of silicene sheets.

Based on the construction of the Voronoi polyhedra, the nearest geometric neighbors in the packings of lithium atoms were identified. Figure 3 shows the distribution of the angles θ of the relative position of these neighbors relative to the centers of the polyhedra. As seen from Fig. 3, the substrate material has a significant effect on the shape of the θ spectra. There are sharp peaks in the θ distributions, which reflect the characteristic ordering of Li atoms. The peaks at the angles $k \times 30°$ and $k \times 45°$, where k is an integer, correspond to an ideal crystal packing [22].

Such a packing appears in the silicene channel when Li atoms are located above hexagonal cells formed by Si atoms. Sharp peaks are much less pronounced when the channels are located on a copper substrate. The intensity of these peaks decreases as the size of vacancy defects in silicene grows. Sharp peaks are significantly more pronounced when the channel is placed on a nickel substrate. This may be mainly due to an increase in the fraction of Li atoms "attached" to hexagonal Si cells, since a change in the total number of Li atoms in the channel (compared with the use of a Cu (111) substrate) does not reduce the intensity of sharp peaks, in the case of a Ni (111) substrate. However, it should be noted that some of the sharp peaks in the θ distribution obtained with the nickel substrate are shifted relative to the locations corresponding to the crystalline packing. This indicates the presence of a significant proportion of irregular packing of Li atoms in the channel. The share of such a packing is especially large in the channels on the Cu (111) substrate, for which the θ distribution has a high irregular background. Important information on the detailed structure of lithium in the silicene channels, obtained after intercalation, is presented in the Online Resource 1. It consists of the data obtained by the statistical geometry method based on the construction of simplified Voronoi polyhedra (SPs).

The stress σ_{zz} generated by a force acting perpendicular to the plane of silicene is the greatest when the channel is filled with lithium when using substrates of either type. The averaged distribution of stresses σ_{zz} over silicene sheets located on Ni (111) and Cu (111) substrates at the time of the maximum filling of the channel with lithium is shown in Fig. 4. Regardless of the presence of defects in

silicene, the local stresses σ_{zz} in the silicene channel on the copper substrate are noticeably higher than the corresponding stresses appearing in the channel on the nickel substrate. Moreover, the maximum values of the σ_{zz} stresses in the silicene channel on the Cu (111) substrate are reached near the entrance of the ion to the channel, when it has not yet lost much of its kinetic energy after colliding with Si and Li atoms. In this case, the highest value of the local stress $\sigma_{zz}^{\max}$ (6.45 GPa) is observed for the perfect silicene channel on the Cu (111) substrate. The resulting stress $\sigma_{zz}^{\max}$ is about 43% of the ultimate tensile stress σ_{zx}^{ult} acting along the zigzag direction in silicene [23]. On a nickel substrate, the highest stress $\left|\sigma_{zz}^{\max}\right|$ (3.27 GPa) is reached when trivacancies are present in the channel walls. The magnitude of this stress does not exceed 21.8% of the value of the σ_{zx}^{ult} stress.

5 Conclusions

The present study showed that both copper and nickel substrate are more preferable candidates when creating the LIB anode material, than the silver substrate. Substrates of copper and nickel have different effects on the capacitance and stress state created during the operation of the silicene anode. The capacity of silicene channels (both perfect and with vacancy defects) on a Ni (111) substrate during lithium intercalation, as a rule, exceeds the capacity of the corresponding Si channel created on the Cu (111) substrate. The resulting maximum stresses in the channel walls on the nickel substrate turn out to be noticeably lower than the similar characteristics accompanying the process of lithium intercalation in the channel on the copper substrate. These factors should be taken into account when producing new advanced materials for the LIB anode.

Acknowledgements This work was supported by the Russian Science Foundation (the Grant Number 16-13-00061).

Compliance with ethical standards

Conflict of interest The authors declare that they have no conflicts of interest.

References

1. Kamali AR, Fray DJ (2011) Tin-based materials as advanced anode materials for lithium ion batteries: a review. Rev Adv Mater Sci 27:14–24
2. Dou F, Shi L, Chen G, Zhang D (2019) Silicon/carbon composite anode materials for lithium-ion batteries. Electrochem Energy Rev 2:149–198. https://doi.org/10.1007/s41918-018-00028-w
3. Ryu J, Hong D, Lee H-W, Park S (2017) Practical considerations of Si-based anodes for lithium-ion battery applications. Nano Res 10(12):3970–4002. https://doi.org/10.1007/s12274-017-1692-2
4. Salah M, Murphy P, Hall CJ, Francis C, Kerr R, Fabretto M (2019) Pure silicon thin-film anodes for lithium-ion batteries: a review. J Power Sources 414:48–67. https://doi.org/10.1016/j.jpowsour.2018.12.068
5. Luo X, Lang J, Lv S, Li Z (2018) High performance sandwich structured Si thin film anodes with LiPON coating. Front Mater Sci 12(2):147–155. https://doi.org/10.1007/s11706-018-0416-1
6. Zamani N, Modarresi-Alam AR, Noroozifar M, Javanbakht M (2019) The improved performance of lithium-ion batteries via the novel electron transport catalytic role of polyaniline (PANI) in PANI/Co_3O_4–CuO raspberry as new anode material. J Appl Electrochem 49(3):327–340. https://doi.org/10.1007/s10800-019-01286-2
7. Wang L, Jia J, Wu Y, Niu K (2018) Antimony/reduced graphene oxide composites as advanced anodes for potassium ion batteries. J Appl Electrochem 48(10):1115–1120. https://doi.org/10.1007/s10800-018-1224-0
8. Kim S-J, Moon S-H, Kim M-C, So J-Y, Han S-B, Kwak D-H, Bae W-G, Park K-W (2018) Micro-patterned 3D Si electrodes fabricated using an imprinting process for high-performance lithium-ion batteries. J Appl Electrochem 48(9):1057–1068. https://doi.org/10.1007/s10800-018-1234-y
9. Li WG, Xu XB, Liu C, Tekell MC, Ning J, Guo JH, Zhang JC, Fan DL (2017) Ultralight and binder-free all-solid-state flexible supercapacitors for powering wearable strain sensors. Adv Funct Mater 27:1702738. https://doi.org/10.1002/adfm.201702738
10. Lu J, Chen Z, Pan F, Cui Y, Amine K (2018) High-performance anode materials for rechargeable lithium-ion batteries. Electrochem Energy Rev 1:35–53. https://doi.org/10.1007/s41918-018-0001-4
11. Balogun MS, Zeng YX, Qiu WT, Luo Y, Onasanya A, Olaniyi TK, Tong YX (2016) Three-dimensional nickel nitride (Ni3N) nanosheets: free standing and flexible electrodes for lithium ion batteries and supercapacitors. J Mater Chem A 4:9844–9849. https://doi.org/10.1039/C6TA02492K
12. Song Y, Xu JL, Liu XX (2014) Electrochemical anchoring of dual doping polypyrrole on graphene sheets partially exfoliated from graphite foil for high-performance supercapacitor electrode. J Power Sources 249:48–58. https://doi.org/10.1016/j.jpowsour.2013.10.102
13. Galashev AE, Zaikov YuP (2015) Computer simulation of Li^+ ion interaction with a graphene sheet. Rus J Phys Chem A 89:2243–2247. https://doi.org/10.1134/S0036024415120122
14. Kawahara K, Shirasawa T, Arafune R, Lin C-L, Takahashi T, Kawai M, Takagi N (2014) Determination of atomic positions in silicone on Ag(111) by low-energy electron diffraction. Surf Sci 623:25–28. https://doi.org/10.1016/jsusc2013.12.013
15. Mazzone AM (2003) Ag deposited onto the (100) surface in silicon studied by density functional theory and classical molecular dynamics. Eur Phys J B 35:517–524. https://doi.org/10.1140/epjb/e2003-00305-2
16. Galashev AY, Ivanichkina KA (2018) Computer study of atomic mechanisms of intercalation/deintercalation of Li ions in a silicene anode on an Ag (111) substrate. J Electrochem Soc 165:A1788–A1796. https://doi.org/10.1149/2.0751809jes
17. Galashev AY, Ivanichkina KA (2019) Computer test of a new silicone anode for lithium-ion battery. ChemElectroChem 6:1525–1535. https://doi.org/10.1002/celc.201900119
18. Plimpton S (1995) Fast parallel algorithms for short-range molecular dynamics. J Comput Phys 117:1–19. https://doi.org/10.1006/jcph.1995.1039

19. Brostow W, Dussault J-P, Fox BL (1978) Construction of Voronoi polyhedral. J Comput Phys 29:81–92. https://doi.org/10.1016/0021-9991(78)90110-9
20. Galashev AE, Elshina LA, Muradymov RV (2016) Molecular dynamic study of the mechanism of formation of 2D carbon nanostructures in a solid Al–C nanocomposite grain. Rus J Phys Chem A 90(12):2444–2448. https://doi.org/10.1134/S0036024416120116
21. Galashev AY (2015) Computer study of the removal of Cu from the graphene surface using Ar clusters. Comput Mater Sci 98:123–128. https://doi.org/10.1016/j.commatsci.2014.11.002
22. Galashev AY (2013) Atomistic simulations of methane interactions with an atmospheric moisture. J Chem Phys 139:124303. https://doi.org/10.1063/1.4821192
23. Chavez-Castillo MR, Rodrıguez-Mezab MA, Meza-Montes L (2015) Size, vacancy and temperature effects on Young's modulus of silicene nanoribbons. RSC Adv 5:96052–96061. https://doi.org/10.1039/C5RA15312C

Affiliations

Alexander Y. Galashev[1,2] · Yuri P. Zaikov[1,2]

[1] Institute of High-Temperature Electrochemistry, Ural Branch, Russian Academy of Sciences, Academic Str. 20, Yekaterinburg, Russia 620990

[2] Ural Federal University, Mira Str., 19, Yekaterinburg, Russia 620002